Cork Open Research Archive
Cartlann Taighde Oscailte Chorcaí

UCC Library and UCC researchers have made this item openly available. Please let us know how this has helped you. Thanks!

Title	Impact of etch processes on the chemistry and surface states of the topological insulator Bi2Se3
Author(s)	Barton, Adam T.; Walsh, Lee A.; Smyth, Christopher M.; Qin, Xiaoye; Addou, Rafik; Cormier, Christopher; Hurley, Paul K.; Wallace, Robert M.; Hinkle, Christopher L.
Publication date	2019-08-15
Original citation	Barton, A. T., Walsh, L. A., Smyth, C. M., Qin, X., Addou, R., Cormier, R., Hurley, P. K., Wallace R. M., and Hinkle (2019) 'Impact of etch processes on the chemistry and surface states of the topological insulator Bi2Se3', ACS Applied Materials & Interfaces, 11 (35), pp.32144-32150. doi: 10.1021/acsami.9b10625
Type of publication	Article (peer-reviewed)
Link to publisher's version	http://dx.doi.org/10.1021/acsami.9b10625 Access to the full text of the published version may require a subscription.
Rights	**© 2019, American Chemical Society. This document is the Accepted Manuscript version of a Published Work that appeared in final form in ACS Applied Materials & Interfaces, copyright © American Chemical Society after peer review and technical editing by the publisher. To access the final edited and published work see https://pubs.acs.org/doi/10.1021/acsami.9b10625**
Item downloaded from	http://hdl.handle.net/10468/12192

Downloaded on 2021-11-27T17:17:45Z

UCC
University College Cork, Ireland
Coláiste na hOllscoile Corcaigh

ACS APPLIED MATERIALS & INTERFACES

Subscriber access provided by UNIV COLL CORK

Functional Inorganic Materials and Devices

Impact of Etch Processes on the Chemistry and Surface States of the Topological Insulator BiSe

Adam Barton, Lee A. Walsh, Christopher M. Smyth, Xiaoye Qin, Rafik Addou, Christopher Cormier, Paul K. Hurley, Robert M. Wallace, and Christopher L Hinkle

ACS Appl. Mater. Interfaces, **Just Accepted Manuscript** • DOI: 10.1021/acsami.9b10625 • Publication Date (Web): 15 Aug 2019

Downloaded from pubs.acs.org on August 21, 2019

Just Accepted

"Just Accepted" manuscripts have been peer-reviewed and accepted for publication. They are posted online prior to technical editing, formatting for publication and author proofing. The American Chemical Society provides "Just Accepted" as a service to the research community to expedite the dissemination of scientific material as soon as possible after acceptance. "Just Accepted" manuscripts appear in full in PDF format accompanied by an HTML abstract. "Just Accepted" manuscripts have been fully peer reviewed, but should not be considered the official version of record. They are citable by the Digital Object Identifier (DOI®). "Just Accepted" is an optional service offered to authors. Therefore, the "Just Accepted" Web site may not include all articles that will be published in the journal. After a manuscript is technically edited and formatted, it will be removed from the "Just Accepted" Web site and published as an ASAP article. Note that technical editing may introduce minor changes to the manuscript text and/or graphics which could affect content, and all legal disclaimers and ethical guidelines that apply to the journal pertain. ACS cannot be held responsible for errors or consequences arising from the use of information contained in these "Just Accepted" manuscripts.

is published by the American Chemical Society. 1155 Sixteenth Street N.W., Washington, DC 20036

Published by American Chemical Society. Copyright © American Chemical Society. However, no copyright claim is made to original U.S. Government works, or works produced by employees of any Commonwealth realm Crown government in the course of their duties.

1
2
3
4
5
6
7
8
9
10
11
12
13
14
15
16
17
18
19
20
21
22
23
24
25
26
27
28
29
30
31
32
33
34
35
36
37
38
39
40
41
42
43
44
45
46
47
48
49
50
51
52
53
54
55
56
57
58
59
60

Impact of Etch Processes on the Chemistry and Surface States of the Topological Insulator Bi_2Se_3

Adam T. Barton,[1,+] Lee A. Walsh,[1,2,+] Christopher M. Smyth,[1] Xiaoye Qin,[1] Rafik Addou,[1]

Christopher Cormier,[1] Paul K. Hurley,[2] Robert M. Wallace,[1] and Christopher L. Hinkle[1,3]*

[1] Department of Materials Science and Engineering, University of Texas at Dallas,

Richardson, TX, 75080, USA

[2] Tyndall National Institute, University College Cork, Lee Maltings Complex, Cork

T12R5CP, Ireland

[3] Department of Electrical Engineering, University of Notre Dame, Notre Dame, IN,

46556 USA

KEYWORDS: Topological Insulator, Bismuth Selenide, Surface States, Process Integration, Dirac Cone, Etch Chemistry

ABSTRACT

The unique properties of topological insulators like Bi_2Se_3 are intriguing for their potential implementation in novel device architectures for low-power, defect-tolerant logic and memory devices. Recent improvements in the synthesis of Bi_2Se_3 has positioned researchers to fabricate new devices to probe the limits of these materials. The fabrication of such devices, of course, requires etching of the topological insulator, in addition to other materials including gate oxides and contacts which may impact the topologically protected surface states. In this paper, we study the impact of He^+-

sputtering and inductively coupled plasma Cl_2 and SF_6 reactive etch chemistries on the physical, chemical, and electronic properties of Bi_2Se_3. Chemical analysis by X-ray photoelectron spectroscopy tracks changes in the surface chemistry and Fermi level, showing preferential removal of Se that results in vacancy-induced n-type doping. Chlorine based chemistry successfully etches the Bi_2Se_3, but with residual Se-Se bonding and interstitial Cl species remaining after the etch. The Se vacancies and residuals can be removed with post-etch anneals in a Se environment, repairing the Bi_2Se_3 nearly to the as-grown condition. Critically, in each of these cases, angle-resolved photoemission spectroscopy (ARPES) reveals that the topologically protected surface states remain even after inducing significant surface disorder and chemical changes, demonstrating that topological insulators are quite promising for defect tolerant electronics. Changes to the ARPES intensity and momentum broadening of the surface states are discussed. Fluorine-based etching aggressively reacts with the film resulting in a relatively thick insulating film of thermodynamically favored BiF_3 on the surface, prohibiting the use of SF_6-based etching in Bi_2Se_3 processing.

1
2
3
4
5
6
7
8
9
10
11
12
13
14
15
16
17
18
19
20
21
22
23
24
25
26
27
28
29
30
31
32
33
34
35
36
37
38
39
40
41
42
43
44
45
46
47
48
49
50
51
52
53
54
55
56
57
58
59
60

INTRODUCTION

Topological insulators (TIs) are a unique class of material that possess narrow, semiconducting "bulk" bandgaps, but also have gapless edge or surface states (in 2D or 3D topological insulators, respectively)[1-3] that are protected by time-reversal symmetry.[4-5] These topologically protected states have their spin locked to the direction of the momentum, potentially enabling spin-polarized current and defect tolerant transport. Bi_2Se_3 is the most widely studied topological insulator and recent progress in the growth of Bi_2Se_3, including the reduction of parasitic bulk conduction caused by point defects,[6] have finally positioned researchers to synthesize unique devices based on the topologically protected states.

During device processing there are often a number of etching and sputtering steps that are used to form and isolate the devices. Although necessary for complex device fabrication, these destructive processes can also have the adverse effect of inducing damage in the underlying materials. Research has shown that the surface states of 3D

TIs are robust to non-magnetic defects and should persist even after significant damage.[7-8] However, there is a limit to this defect tolerance. Previous studies have shown that at some critical defect concentration, the disorder in the near-surface region can significantly alter the band structure, effectively forming a different material at the extreme limit, and causing the surface states to recede to the next topmost quintuple layer (in the case of 3D TIs).[9-11] Before Bi_2Se_3 can be integrated into process flows that include etching steps, the effects of process-induced damage must be understood.

While there have been a few studies focused on the impact of (non-magnetic) defects on the surface states of TIs, those studies did not investigate specifically how the damage impacts the structure and chemistry of the surface.[12-13] Furthermore, there have been no publications on the impact of dry-etching Bi_2Se_3 with reactive precursors that are common in advanced device processing. Due to the ease of sputtering through van der Waals chalcogenides with ionized noble gasses, we first investigate the impact of Bi_2Se_3 damaged by He^+ ion sputtering. If Bi_2Se_3 is utilized in a van der Waals heterostructure, ionized sputtering with noble gasses may be sufficient for shaping the

1 2 3 4 5 6 7 8 9 10 11 12 13 14 15 16 17 18 19 20 21 22 23 24 25 26 27 28 29 30 31 32 33 34 35 36 37 38 39 40 41 42 43 44 45 46 47 48 49 50 51 52 53 54 55 56 57 58 59 60

device features. However, if more robust materials are utilized in the device structure (i.e. Fe, Co, Ni, etc.), it may be necessary to use more reactive etching processes.[14-16] Therefore, the use of inductively-coupled plasma (ICP) etching using Cl_2 and SF_6 reactive species was also investigated. Using angle-resolved photoemission spectroscopy (ARPES), X-ray photoelectron spectroscopy (XPS), scanning-tunneling spectroscopy (STS), and atomic force microscopy (AFM) we investigate the surface chemistry, physical damage, and changes in electronic structure induced by these destructive processes and provide a guide for minimizing and, in some cases, even reversing some of the adverse effects.

EXPERIMENTAL METHODS

Molecular Beam Epitaxial Growth of Bi_2Se_3

50 nm thick Bi_2Se_3 was grown on c-plane sapphire substrates using a two-step MBE process described in detail elsewhere.[4,17] The quality of the MBE grown material is highly reproducible, and full characterization of the grown material has been repeated for several growths, where near identical grain size of 2 μm, crystallinity, and chemical

composition is observed in all cases. Diffraction indicates a highly ordered film with slight azimuthal intergranular mismatch and some twinned domains.

Samples for *ex-situ* XPS, ARPES, and STS analysis were Se capped at room temperature for 1 hour *in-situ* after growth, to achieve a capping layer ~40 nm thick. This was used to prevent oxidation and the adsorption of environmental contaminants on the Bi_2Se_3 surface during transfer to the XPS, ARPES, or STS instruments. Desorption of the protective cap was performed by thermal anneal at 170°C for 30 min under a base pressure of 10^{-9} mbar in the instruments.

Sputter Process

Sputtering was performed using a He^+ ion beam at 1 keV (the lowest energy available on this system for controlled sputtering) for either 45 min or 135 min *in-situ* in the same chamber as the XPS instrument. The etch was performed by rastering the sputter gun beam over an area of 6x6 mm^2. This then allows the XPS analysis (with a spot size of 0.5 mm^2) to be performed over the sputtered region without picking up signal from the non-sputtered Bi_2Se_3.

1 2 3 4 5 6 7 8 9 10 11 12 13 14 15 16 17 18 19 20 21 22 23 24 25 26 27 28 29 30 31 32 33 34 35 36 37 38 39 40 41 42 43 44 45 46 47 48 49 50 51 52 53 54 55 56 57 58 59 60

Etch Process

The ICP etch process was performed in a Plasma-Therm ICP Etcher at room temperature with reactive species of either SF_6 or Cl_2. The samples that underwent ICP etching were never capped due to the lack of controlled heating in the etch tool. The uncapped samples were placed into the etch tools within 5 minutes of removal from the growth chamber. The flourine–based etch recipe used 10 sccm of SF_6, 5 sccm of Ar, with a forward power of 100 W, and a forward bias of 50 W. The chlorine-based etch recipe used 10 sccm of Cl_2, 5 sccm of Ar, 100 W forward power, and 50 W forward bias. In both cases there was a 10 s stabilization step, a 5 s plasma ignition step, and a constant etch lasting 5 s. These reactive chemistries were chosen due to their widespread use in the industrial etching of dielectric and ferromagnetic films,[14-16] and therefore, fully understanding their impact on the Bi_2Se_3 surface chemistry is necessary for the further application in advanced device processing. Although Bi_2Se_3 is easily etched with inert processes, integration in novel device architectures will expose Bi_2Se_3

1
2
3
4
5
6
7
8
9
10
11
12
13
14
15
16
17
18
19
20
21
22
23
24
25
26
27
28
29
30
31
32
33
34
35
36
37
38
39
40
41
42
43
44
45
46
47
48
49
50
51
52
53
54
55
56
57
58
59
60

to reactive sputtering processes involved in sputtering through more physically robust layers.

After the sputter process, the ARPES samples were transferred *ex-situ* back to the MBE chamber in the minimum time (<10 min) in order to again cap them with Se to ensure the surface is protected during transfer to the ARPES system (which is located at the SLAC National Accelerator Laboratory).[18] The samples for ARPES analysis were cleaved from this damaged region to a size of ~2x2 mm^2. The same decapping procedure as previously mentioned was used in the ARPES preparation chamber to recover the bare Bi_2Se_3 surface. For the XPS characterization of the ICP-etched films (the XPS tool is in the same building as the ICP etchers at UT Dallas), the samples were transferred directly from the ICP etcher to the XPS system, while allowing the same amount of atmospheric exposure as the ARPES samples. This resulted in minor atmospheric oxidation.[6]

XPS Characterization and Peak Fitting

XPS for all samples (except the SF_6-etched sample as described later) was carried out using a monochromated Al Kα source (E = 1486.7 eV) and an *Omicron* EA125 hemispherical analyzer with resolution of ±0.05 eV. The analyzer acceptance angle of 8°, takeoff angle of 45°, and pass energy of 15 eV were utilized in this study. This tool is described in detail elsewhere.[20] The analyzer was calibrated using sputter cleaned Au, Cu, and Ag foils, as is outlined in ASTM E2108. The stoichiometries extracted from XPS are calculated using the appropriate relative sensitivity factors for the Bi 5*d*, Se 3*d*, O 1*s*, Cl 2*p*, F 1*s*, and S 2*s* core levels (1.259, 0.722, 0.711, 0.77, 1.000, and 0.399, respectively).[21] The stoichiometry ratios calculated are accompanied by a ±0.2 error.

Due to the need for a charge neutralizer, the XPS for the SF_6-etched sample was scanned in an *Omicron* ultra-high vacuum (UHV) system equipped with STM and XPS running at a base pressure of ~1 × 10^{-10} mbar. A monochromatic Al *Kα* source (*E* = 1486.7 eV) and an *Omicron Argus* detector operating with pass energy of 15 eV have been used with a spot size of 630 μm^2. The analyzer spectrometer energy scale was calibrated using sputter cleaned Au, Ag, and Cu specimens as indicated in the ASTM

1 2 3 4 5 6 7 8 9 10 11 12 13 14 15 16 17 18 19 20 21 22 23 24 25 26 27 28 29 30 31 32 33 34 35 36 37 38 39 40 41 42 43 44 45 46 47 48 49 50 51 52 53 54 55 56 57 58 59 60

E2108 procedure. The core level spectra were deconvoluted using the curve-fitting software AAnalyzer.[22] Metallic chemical states were fit with the asymmetric double Lorentzian line shape, while non-metallic chemical states were fit with Voigt line shapes. An active Shirley background subtraction was employed in fitting all spectra.[22] In order to accurately detect the presence of additional features in any of the core levels, all fits were performed with comparison to reference samples, i.e. using the bare Bi_2Se_3 after removal of the Se cap, and oxidized Bi_2Se_3 after one week of atmospheric exposure. The peak separations and full-width half-maxima (FWHM) of the reference peaks are kept constant to maintain consistency.

STS Characterization

Room temperature scanning tunneling spectroscopy (STS) spectra were obtained using a VT-STM with an etched tungsten tip in the *Omicron* UHV system. STS data were collected at a single position and averaged from at least 30 sweeps to obtain a single curve.[23] Then, a direct differentiation of the I–V curves was plotted in linear or log scale.

ARPES Measurements

ARPES measurements were performed at beamline 5-4 of the Stanford Synchrotron Light Source (SSRL) with a *Scienta R4000* electron analyzer.[18] All of the data shown was acquired using 23 eV photon energy with total energy and angular momentum resolutions of 10 meV and 0.25°, respectively. The decapping process was accomplished by heating the samples to 170 °C in UHV for 1 h. The temperatures during measurement were acquired close to the sample position with an accuracy of ±2 °C. The samples were then cooled down to room temperature before transfer to the ARPES analysis chamber. The ARPES measurements were performed at 20 K in a UHV chamber with a base pressure better than 4 x 10^{-11} mbar. Measurements on each sample were completed within less than 10 hours of Se cap removal.

Post Sputter/Etch Se Anneals

The samples etched with the Cl_2/Ar precursors were reintroduced into the MBE chamber used for growth and annealed under a Se flux pressure of 4.5 x 10^{-7} mbar at a temperature of 250°C for one hour. The base pressure was maintained below 1 x 10^{-9} mbar during the anneal, and the sample was transferred to the XPS system immediately

1
2
3
4
5
6
7
8
9
10
11
12
13
14
15
16
17
18
19
20
21
22
23
24
25
26
27
28
29
30
31
32
33
34
35
36
37
38
39
40
41
42
43
44
45
46
47
48
49
50
51
52
53
54
55
56
57
58
59
60

after growth without Se-capping. The transferring of samples was timed such that each sample used for comparison saw the same amount of atmospheric exposure (< 10 min).

RESULTS AND DISCUSSION

He+ Sputter Damage

An XPS study was performed to investigate the change in surface chemistry caused by the He^+-sputtering process. The fitted XPS spectra of the Bi 5*d* and Se 3*d* core levels of the Bi_2Se_3 samples as a function of sputter damage are shown in Figure 1(a,b). The surface of the 0 min sample was scanned directly after the *in-situ* removal of the Se cap and shows the expected chemical states related to Bi_2Se_3 in both core levels. The two peaks observed in the Bi 5*d* and Se 3*d* spectra are due to the spin-orbit split Bi 5*d* (the $5d_{5/2}$ and $5d_{3/2}$ peaks) and Se 3*d* (the $3d_{5/2}$ and $3d_{3/2}$ peaks) doublets and are in good agreement with previous reports.[6,19] After exposure to the He^+ ions for 45 min, the Bi 5*d* core level peak shifts to higher binding energy (BE) by 0.05 eV, suggesting n-type doping of the film. This shift is a result of the sputter process preferentially removing Se from the surface region, discussed in a previous publication.[6] Se vacancies are a well-

known n-type intrinsic dopant in Bi_2Se_3. There are also two additional features that emerge at 24.52 eV and 24.01 eV which are consistent with Se-deficient Bi_2Se_{3-x} and metallic Bi (Bi^0),[24] respectively. These peaks are highlighted in the magnified image, and is again consistent with the removal of Se. After the longer He+ sputter process (135 min) there is a further 0.09 eV shift to higher BE and the Bi^0 feature increases in intensity by a factor of 10. This suggests the continued removal of Se from the surface. The Se 3*d* core level exhibits shifting similar to the Bi 5*d*, but with a slightly different magnitude. This is because the BE shift is the summation of the overall Fermi level shift along with the stoichiometric change of the film. Therefore, a larger shift of 0.14 eV to higher BE is initially observed for the Se 3*d* core level after the 45 min sputter and an additional shift of 0.07 eV after 135 min. As a result of the utilization of the amorphous Se cap, there are no detectable oxygen or carbon signals in any of the samples.

The change in stoichiometry of the surface region was calculated using the areas obtained from the fitted XPS data (sampling depth of 9.8 nm and 9.7 nm for the Bi 5*d* and Se 3*d*, respectively).[25] Figure 1(c) shows the film stoichiometry as a function of

1
2
3
4
5
6
7
8
9
10
11
12
13
14
15
16
17
18
19
20
21
22
23
24
25
26
27
28
29
30
31
32
33
34
35
36
37
38
39
40
41
42
43
44
45
46
47
48
49
50
51
52
53
54
55
56
57
58
59
60

sputter time. As the sputter time increases, the film becomes more Se-deficient, i.e. the sputter damage preferentially removes Se from the surface. This is consistent with the observation of Bi^0 and Bi_2Se_{3-x} and is also consistent with the low evaporation energy of Se (95.5 kJ/mol) compared to Bi (179.0 kJ/mol).[25]

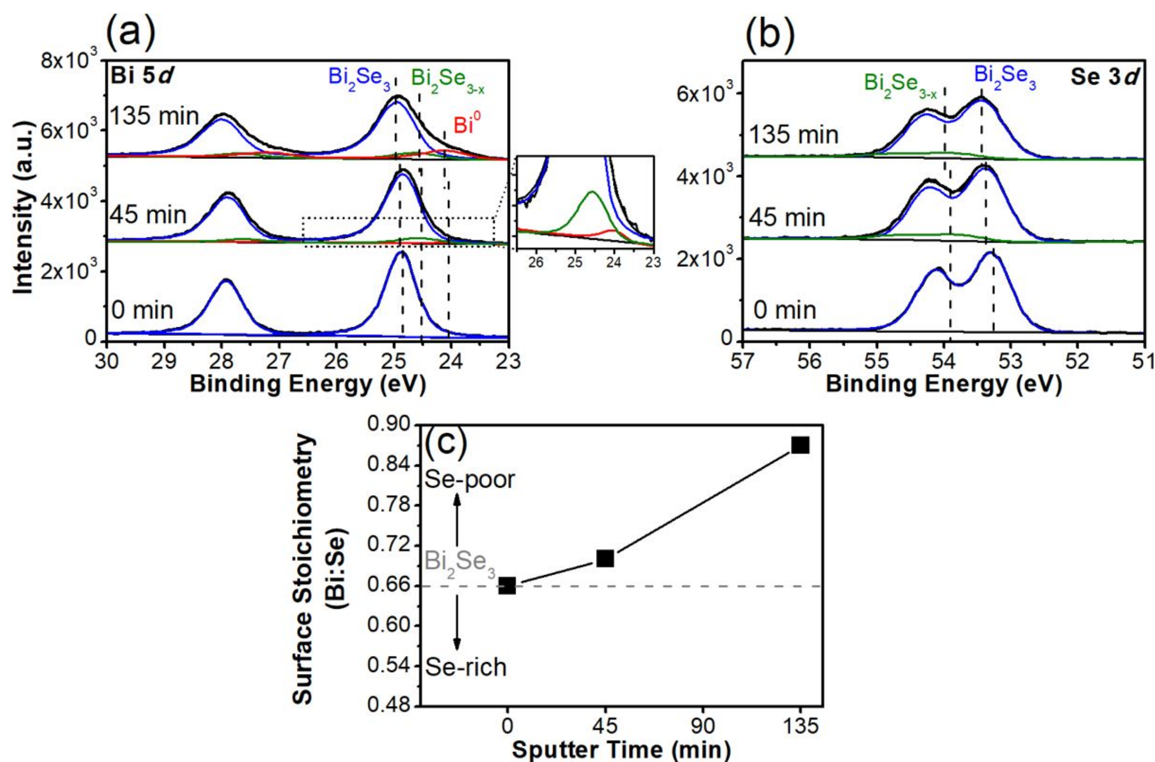

Figure 1: Fitted XPS spectra of (a) the Bi 5*d* core level as a function of increasing sputter time showing the presence of additional states at lower BE. (b) The Se 3*d* core level with an additional high BE state corresponding to Se-poor Bi_2Se_{3-x} after sputter. (c)

1
2
3
4
5
6
7
8
9
10
11
12
13
14
15
16
17
18
19
20
21
22
23
24
25
26
27
28
29
30
31
32
33
34
35
36
37
38
39
40
41
42
43
44
45
46
47
48
49
50
51
52
53
54
55
56
57
58
59
60

A plot showing the Bi:Se stoichiometry as a function of sputter time calculated from XPS.

Figure 2 shows the ARPES spectra of the 50 QL thick Bi_2Se_3 films as a function of sputter time. In each case, the surface states are still detectable regardless of the chemistry changes. However, there are differences in the E-k data. All of the data were acquired along the $\underline{\Gamma} - \underline{K}$ direction. Two different normalization procedures were used to provide insight into the evolution of the band structure as a function of sputter damage. In Figures 2(a-c) the spectra were normalized to the intensity at the Dirac point. This assumes that the defect-tolerant surface states are minimally perturbed by the processing due to the topological protection. Using this normalization method, the surface states can clearly be observed in all three samples with some noticeable momentum broadening of the Dirac cone. Furthermore, the variation in relative intensity between the Dirac point and the bulk bands results in significantly different maximum intensities between the non-sputtered and sputtered films likely due to the slight damage of the topmost quintuple layer of the 45 min sputter film. However, after an

1
2
3
4
5
6
7
8
9
10
11
12
13
14
15
16
17
18
19
20
21
22
23
24
25
26
27
28
29
30
31
32
33
34
35
36
37
38
39
40
41
42
43
44
45
46
47
48
49
50
51
52
53
54
55
56
57
58
59
60

extra 90 min of sputter time, the topmost quintuple layer is likely completely changed/amorphous which attenuates the Dirac cone signal that now comes from the topmost crystalline layer which is now below the surface. This helps explain the loss of definition of the bulk valence band (M-shaped band at -0.6 eV) observed in Figure 2(b).

In Figures 2d-f the same spectra were normalized to the bulk conduction bands at a point 0.05 eV below the Fermi level (-0.05 eV in Figure 2). This method assumes that the bulk band intensity remains constant regardless of sputter damage and provides insight into the variation in surface state intensity detected at the topmost surface. It should be noted that the Fermi level shifts to lower binding energy (n-type doping) as a function of ARPES acquisition time. This is an effect known as “photon induced band bending” and is commonly observed in ARPES measurements.[26] This provides a small level of variability in the normalization procedure, but does not significantly impact the quantitative analysis. Using this normalization method, the Dirac cone again remains detectable in all three samples, although there are noticeable changes in their intensity. After the 45 min sputter, a ~13% reduction in the Dirac cone intensity is observed. After

1
2
3
4
5
6
7
8
9
10
11
12
13
14
15
16
17
18
19
20
21
22
23
24
25
26
27
28
29
30
31
32
33
34
35
36
37
38
39
40
41
42
43
44
45
46
47
48
49
50
51
52
53
54
55
56
57
58
59
60

135 min of sputter damage, the surface states are still detectable but experience a ~51% decrease in Dirac cone intensity. As with the previous normalization method, this is consistent with the 45 min sputter sample having some damage to the top QL, while the 135 min sputter sample exhibits an amorphous surface layer attenuating the signal from the underlying crystalline quintuple layer.

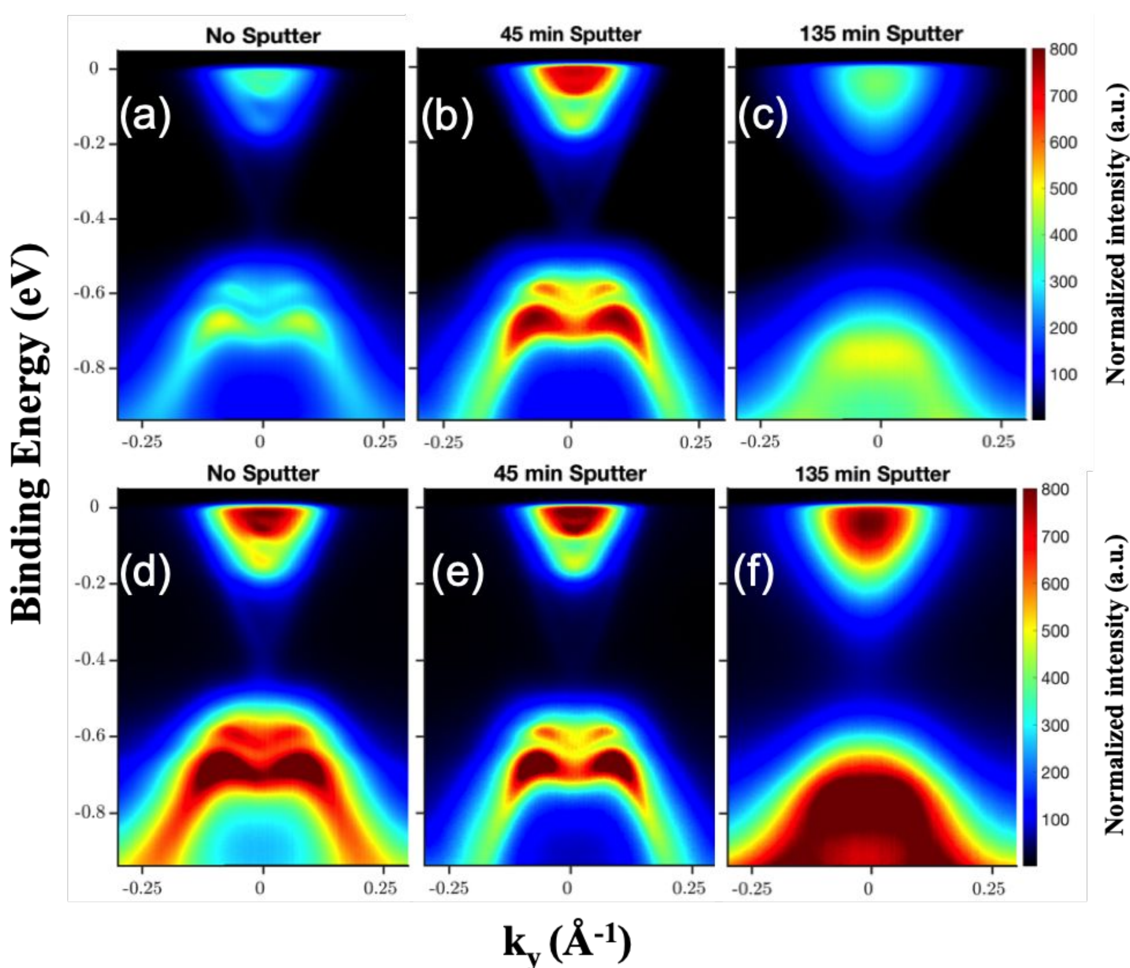

1
2
3
4
5
6
7
8
9
10
11
12
13
14
15
16
17
18
19
20
21
22
23
24
25
26
27
28
29
30
31
32
33
34
35
36
37
38
39
40
41
42
43
44
45
46
47
48
49
50
51
52
53
54
55
56
57
58
59
60

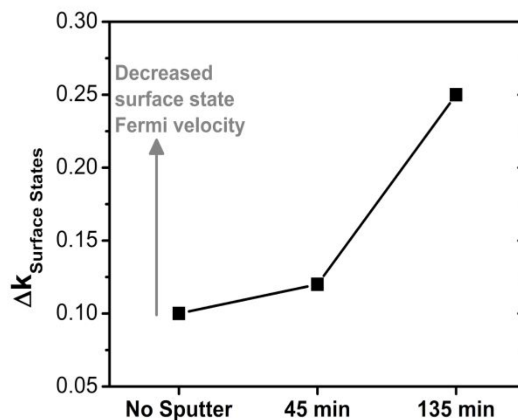

Figure 2: ARPES spectra acquired along the $\underline{\Gamma} - \underline{K}$ direction for (a) as-grown Bi_2Se_3, (b)

Bi_2Se_3 which has undergone He+ ion sputtering for 45 min, and (c) Bi_2Se_3 which has undergone the same sputtering process for 135 min. These spectra are normalized to the Dirac point. The surface state Dirac cone is observable in all three spectra. The bulk band structure also becomes less distinct in the heavy sputter case. The same spectra are shown in (d), (e) and (f), this time normalized to the intensity at -0.05 eV, in the bulk conduction band.

1
2
3
4
5
6
7
8
9
10
11
12
13
14
15
16
17
18
19
20
21
22
23
24
25
26
27
28
29
30
31
32
33
34
35
36
37
38
39
40
41
42
43
44
45
46
47
48
49
50
51
52
53
54
55
56
57
58
59
60

Figure 3: The surface state widths (Δk_{SS}) slightly above the Dirac point, as extracted from the ARPES spectra.

The changes in the surface chemistry/crystallinity results in a broadening of the Dirac cone.[27] Figure 3 shows the extracted surface state momentum width (Δk_{SS}) for each sample, measured at 0.01 eV above the Dirac point. The Dirac cone diameter, measured to be 0.10 Å^{-1} for the undamaged sample, increases by 20% after the 45 min sputter to 0.12 Å^{-1}, and a further 108% increase after the 135 min sputter to 0.25 Å^{-1}. This momentum broadening corresponds to a decreased surface state Fermi velocity and a concomitant increased density of states.

ICP Chemical Etching

To further test the robust nature of the topologically protected surface states of Bi_2Se_3 for novel device integration, ARPES data for the ICP-etched samples was also collected. We note here that significant charging was observed for the SF_6-etched sample and prevented any ARPES data collection (due to the formation of insulating BiF_3 as will be described later). Figure 4(b) shows the result for the Cl_2-etched sample

1
2
3
4
5
6
7
8
9
10
11
12
13
14
15
16
17
18
19
20
21
22
23
24
25
26
27
28
29
30
31
32
33
34
35
36
37
38
39
40
41
42
43
44
45
46
47
48
49
50
51
52
53
54
55
56
57
58
59
60

normalized to the conduction band, where the electronic structure closely resembles the 45 min He^+-sputtered sample shown in Figure 2(e). Again, this indicates light damage to the topmost quintuple layer of Bi_2Se_3. Furthermore, similar momentum broadening to 0.12 $Å^{-1}$ (20%) at 0.01 eV above the Dirac point for the Cl_2-etched sample is observed. We note that the 45 min He+ sputtered sample and the Cl_2-etched sample have nearly identical perturbed surface stoichiometries (Fig. 1(c) and Fig. 5(d)) and nearly identical Dirac cone broadening. When the damage is more severe (and the surface stoichiometry change is greater) as in the 135 min He+ sputtered sample, the broadening is also more severe. The amount of broadening does not appear to depend on the actual process by which the damage occurs, just the extent of the damage.

1
2
3
4
5
6
7
8
9
10
11
12
13
14
15
16
17
18
19
20
21
22
23
24
25
26
27
28
29
30
31
32
33
34
35
36
37
38
39
40
41
42
43
44
45
46
47
48
49
50
51
52
53
54
55
56
57
58
59
60

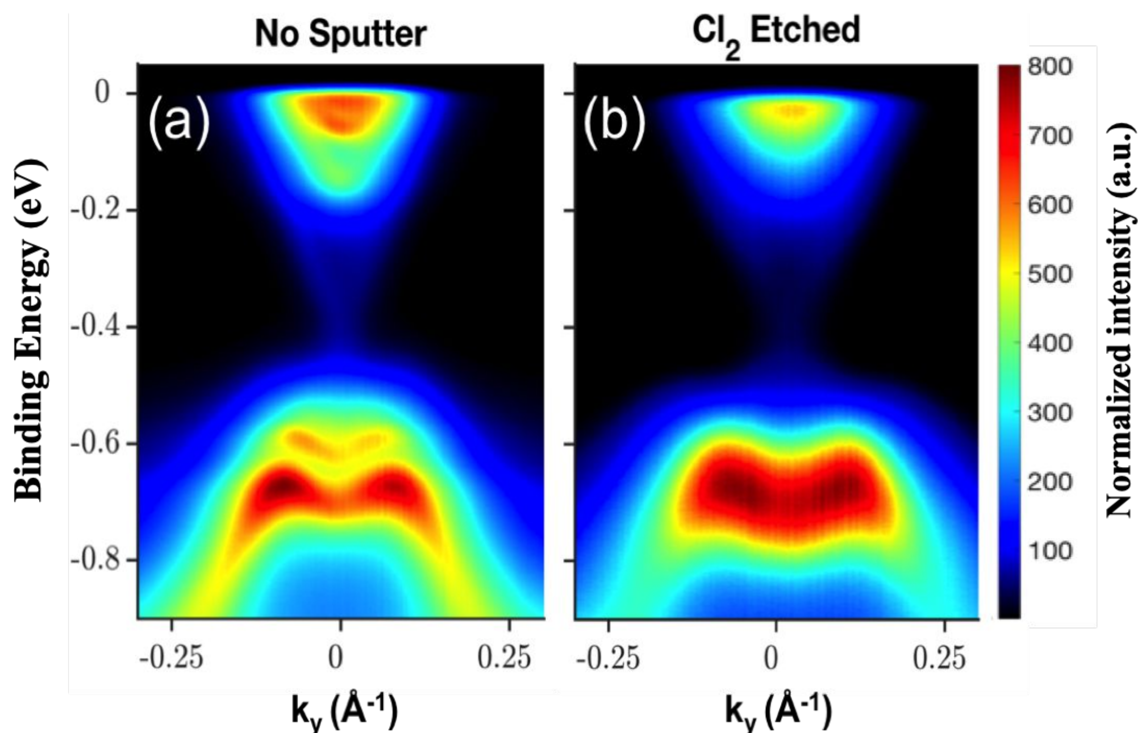

Figure 4: ARPES data of the (a) non-sputtered Bi_2Se_3 and (b) Cl_2-etched Bi_2Se_3 along the $\underline{\Gamma} - \underline{K}$ direction showing that the Dirac cone remains post-etch.

Figure 5: Fitted and normalized XPS data showing the (a) Bi 5*d* and (b) Se 3*d* core levels for the as-grown Bi_2Se_3, the Cl_2-etched, and the SF_6-etched samples. The significant changes in binding energy and chemical states reflect the vast differences in reactivity between Cl and F ions with Bi_2Se_3. (c) F 1*s* core level for the SF_6-etched

1
2
3
4
5
6
7
8
9
10
11
12
13
14
15
16
17
18
19
20
21
22
23
24
25
26
27
28
29
30
31
32
33
34
35
36
37
38
39
40
41
42
43
44
45
46
47
48
49
50
51
52
53
54
55
56
57
58
59
60

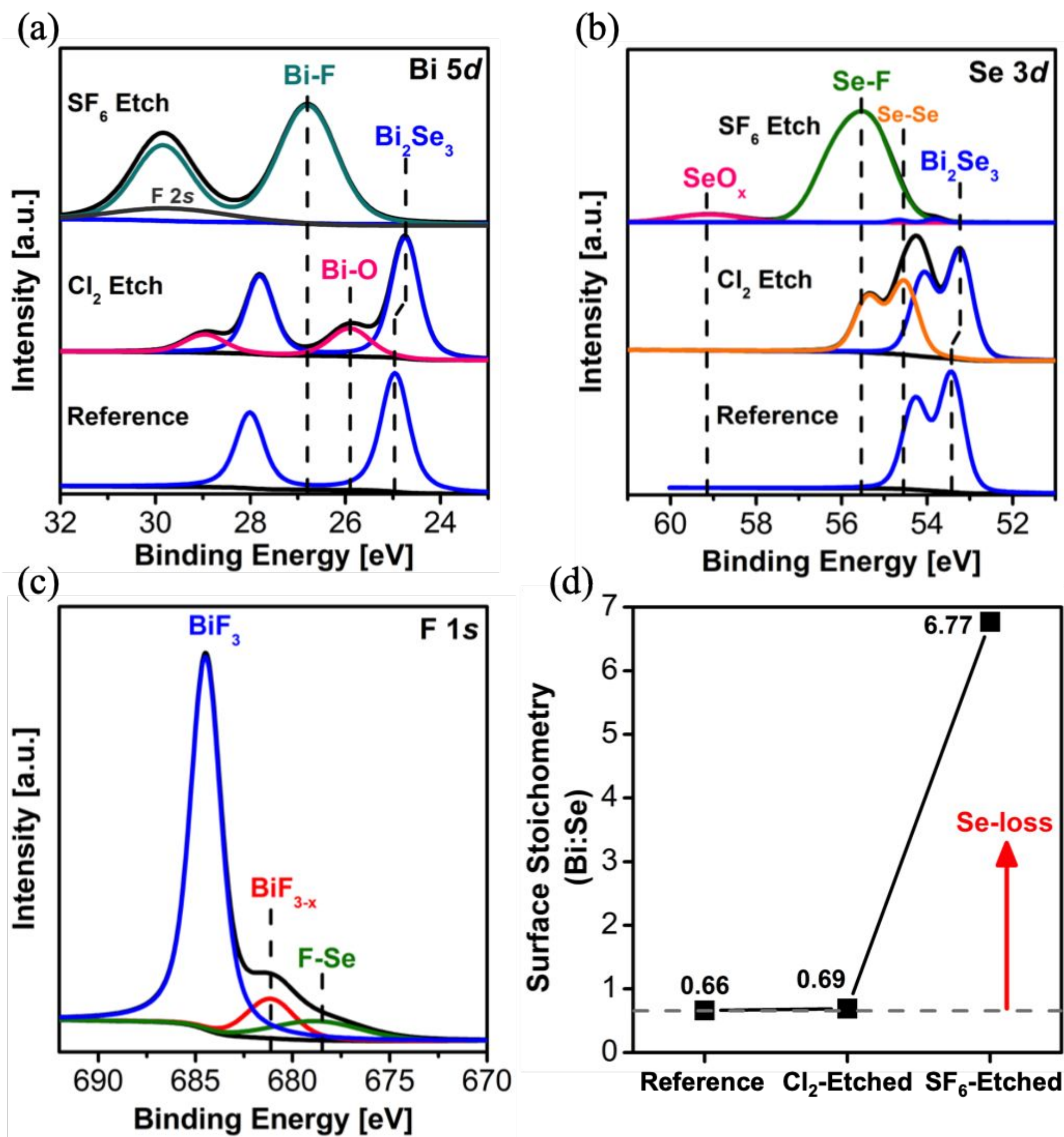

sample. (d) Surface stoichiometry as determined from XPS, highlighting the drastic loss of Se for the SF_6-etched sample.

A complementary XPS study was performed to investigate the change in surface chemistry following the ICP etch process. Figures 5(a,b) show the Bi 5*d* and Se 3*d* core levels obtained immediately after etching, with roughly 10 min of atmospheric exposure required to load the samples into the XPS system. For the Cl_2-etched sample, the Bi 5*d* core level exhibits a Bi-O feature at 25.89 eV and lacks a chemical state related to Bi-Cl bonds. This likely results from the preferential removal of selenium during the Cl_2 etch and an energetically favorable reaction with atmospheric oxygen over ionized chlorine (338.9±5.9 kJ/mol compared to 300.4±4.2 kJ/mol, respectively).[28] When compared to a reference Bi_2Se_3 sample, the Bi_2Se_3 core level shifts 0.19 eV to lower binding energy. This is consistent with the shift in the XPS measured valence band offset, and indicates p-type doping, possibly through intercalated chlorine radicals as has been previously observed for bi- and tri-layer graphene. The Se 3*d* core level associated with Bi_2Se_3 also shifts to lower binding energy as shown in Figure 5(b). Furthermore, a second doublet can be observed that is consistent with amorphous Se-Se surface species.

1
2
3
4
5
6
7
8
9
10
11
12
13
14
15
16
17
18
19
20
21
22
23
24
25
26
27
28
29
30
31
32
33
34
35
36
37
38
39
40
41
42
43
44
45
46
47
48
49
50
51
52
53
54
55
56
57
58
59
60

Significant charging was again observed for the SF_6-etched sample, and a charge neutralizer had to be utilized to gather reliable data. In stark contrast to the Cl_2-etched sample, the SF_6-etched sample shows severe Se loss and the formation of a new Bi-F chemical state. In both the Bi 5*d* and Se 3*d* core levels, the Bi_2Se_3 chemical states are almost completely eliminated and replaced with Bi-F and Se-F states, respectively. This is likely due to the more energetically favorable Bi-F bond (366.5±12.5 kJ/mol compared to 280.3±5.9 kJ/mol for Bi-Se).[29] The attenuation of the Bi_2Se_3 indicates that the new Bi-F overlayer is 7-10 nm thick. Stoichiometry calculations reveal a Bi:F atomic ratio of ~0.28, and indicate the formation of BiF_3. BiF_3 is an insulator with a bandgap of 5.1 eV, and the formation of a strong insulator on the surface is in agreement with the charging effect observed during ARPES data collection. Further physical analysis of the surface was performed with AFM and can be seen in Figure 6. Figure 6(a) shows a high density of grain boundaries along the surface in the non-sputtered Bi_2Se_3 sample, which may allow the F ions to penetrate into the film and react with the less-stable grain boundaries. This etching mechanism can lead to the rapid replacement of Bi-Se bonds for more energetically favorable Bi-F.

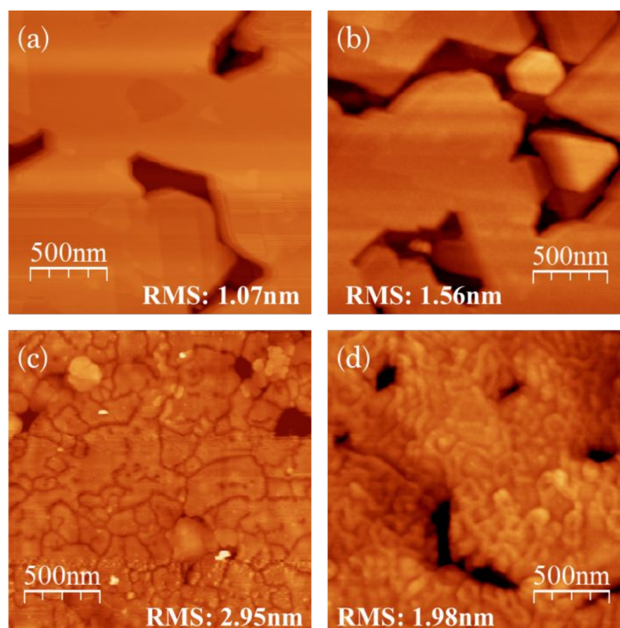

Figure 6: 2x2 μm^2 AFM images of Bi_2Se_3 after (a) growth, (b) 45 min He^+ sputter, (c) 5 s Cl_2 ICP etch, and (d) 5 s SF_6 ICP etch.

Treatments for repairing surface damage

Previous results suggest that Se capping of chacogenide films can fill vacancies and positively impact electronic properties.[29] Here, experiments were performed to interrogate this effect in the near-surface chemistry and Fermi level. To achieve this, a Se-capped Bi_2Se_3 sample was decapped in the XPS system at 170 °C and scanned before sputtering. The sample was then sputtered, with He^+-ions for 45 min, replicating the previously described experiments and interrogated with XPS. Figures 7(a,b) show

1
2
3
4
5
6
7
8
9
10
11
12
13
14
15
16
17
18
19
20
21
22
23
24
25
26
27
28
29
30
31
32
33
34
35
36
37
38
39
40
41
42
43
44
45
46
47
48
49
50
51
52
53
54
55
56
57
58
59
60

the deconvoluted Bi 5*d* and Se 3*d* core level spectra of the sample. A near identical behavior to that in Figure 1 is observed for the 45 min sputter sample, with the Bi_2Se_3 features shifting to higher BE by 0.07 eV and 0.11 eV for the Bi 5*d* and Se 3*d*, respectively. Additionally, the Bi^0 and Bi_2Se_{3-x} features are observed after sputtering, highlighted in the Bi 5*d* inset.

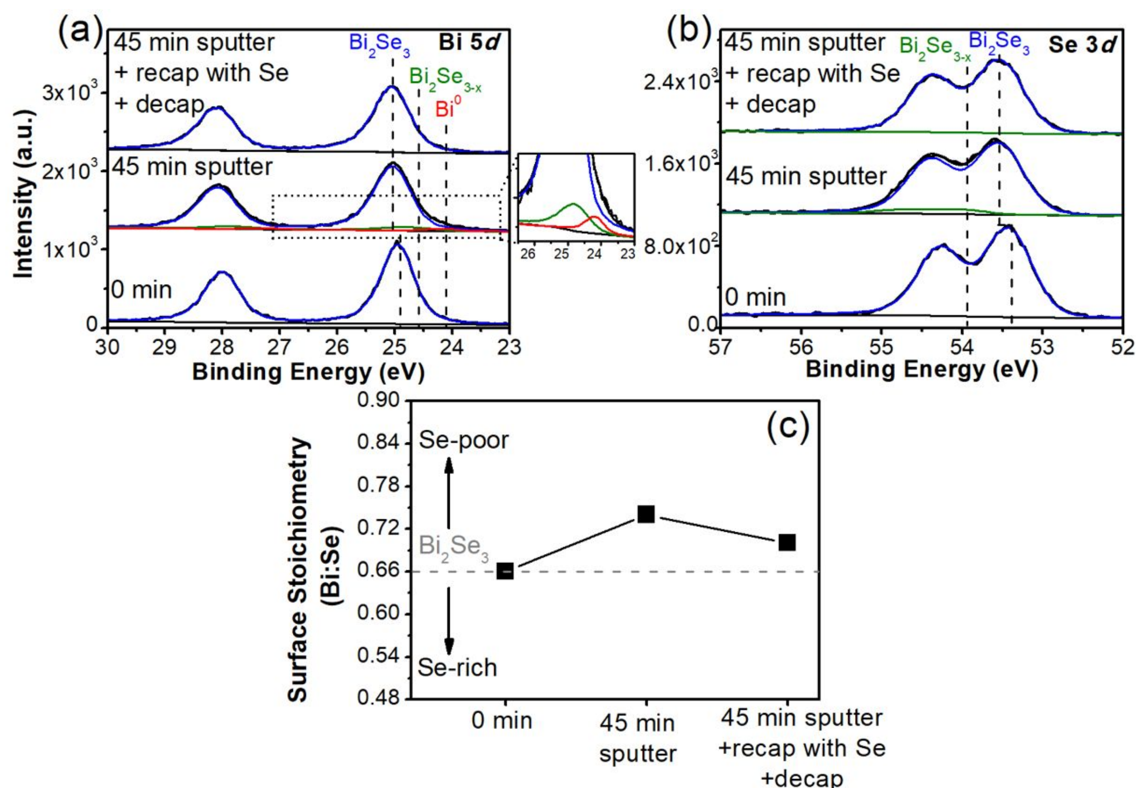

Figure 7: Fitted XPS spectra of (a) the Bi 5*d* core level of a bare sample, the same sample after 45 min sputter time, and the same sample after being capped with Se

1
2
3
4
5
6
7
8
9
10
11
12
13
14
15
16
17
18
19
20
21
22
23
24
25
26
27
28
29
30
31
32
33
34
35
36
37
38
39
40
41
42
43
44
45
46
47
48
49
50
51
52
53
54
55
56
57
58
59
60

again and the cap removed. The previously observed Bi^0 and Bi_2Se_{3-x} states (highlighted in the zoomed inset) are observed after sputtering but are not detectable after re-capping with Se. (b) The Se 3*d* core level showing the presence of Bi_2Se_{3-x} after sputter damage and the reduction of this peak after recapping with Se. (c) A plot showing the stoichiometry extracted from the XPS peak areas as a function of experimental step.

The sample was then re-capped with Se in the MBE system, and then de-capped again in the XPS system at 170 °C. XPS was then immediately performed. All of this reflects the conditions that the ARPES samples, shown previously, were exposed to. In these samples, the Bi^0 and Bi_2Se_{3-x} features decrease from a combined 11% of the total Bi 5*d* area in the 45 min sputter sample, to below the detection limit after the extra cap/decap process. Figure 7(c) shows the film stoichiometry obtained using the same method as Figure 1(c). A slightly higher degree of Se loss occurs in the 45 min sputter sample compared to Figure 1(c), due to sample-to-sample variation. However, following the re-capping procedure, the XPS integrated intensities revert close to their initial levels,

1 2 3 4 5 6 7 8 9 10 11 12 13 14 15 16 17 18 19 20 21 22 23 24 25 26 27 28 29 30 31 32 33 34 35 36 37 38 39 40 41 42 43 44 45 46 47 48 49 50 51 52 53 54 55 56 57 58 59 60

indicating that annealing in the presence of the Se cap causes some of the Bi_2Se_{3-x} and Bi metal to convert back to Bi_2Se_3. This result suggests a possible route to repair damaged or defective Bi_2Se_3 surfaces, and also explains why the ARPES spectra do not show any noticeable contributions from metallic Bi in the sputter damaged samples.

Finally, a study was performed to test this "healing" effect using an alternative method where the samples are annealed at low temperature in a Se background (not capped). For consistency, Bi_2Se_3 films were grown using the same procedure as previously described and exposed to atmospheric conditions for less than 10 minutes when transferring to and from the XPS system. Two Bi_2Se_3 samples were etched using the same ICP parameters as described previously for the Cl_2-etched samples. Immediately following the etch procedure, one sample was transferred to the XPS system for interrogation, and the other was transferred to the MBE system, minimizing atmospheric exposure. The sample in the MBE system was then exposed to a Se flux pressure of 3.5×10^{-7} mbar at 250 °C for 1 hour. The sample was then transferred to the XPS system and the surface chemical states were analyzed for comparison to the pre-anneal

1
2
3
4
5
6
7
8
9
10
11
12
13
14
15
16
17
18
19
20
21
22
23
24
25
26
27
28
29
30
31
32
33
34
35
36
37
38
39
40
41
42
43
44
45
46
47
48
49
50
51
52
53
54
55
56
57
58
59
60

results. Figure 8 shows the Bi 5*d* and Se 3*d* core levels, and the extracted Bi:Se ratios. Following the anneal, the Bi:Se surface stoichiometry recovered toward the intrinsic ratio, indicating the Se-rich anneal resulted in the filling of Se vacancies. The Bi 5*d* core level experienced a 35% reduction in the Bi-O feature as well as a 0.06 eV shift to higher binding energy for the Bi_2Se_3 doublet. The Se 3*d* core level also exhibits a similar shift to higher binding energy for the Bi_2Se_3 doublet, as well as the complete removal of the Se-Se surface species, indicating a change in surface chemistry along with a slight Fermi level shift. However, Figure 8(c) shows that Cl species are still detectable by XPS, even after the Se anneal.

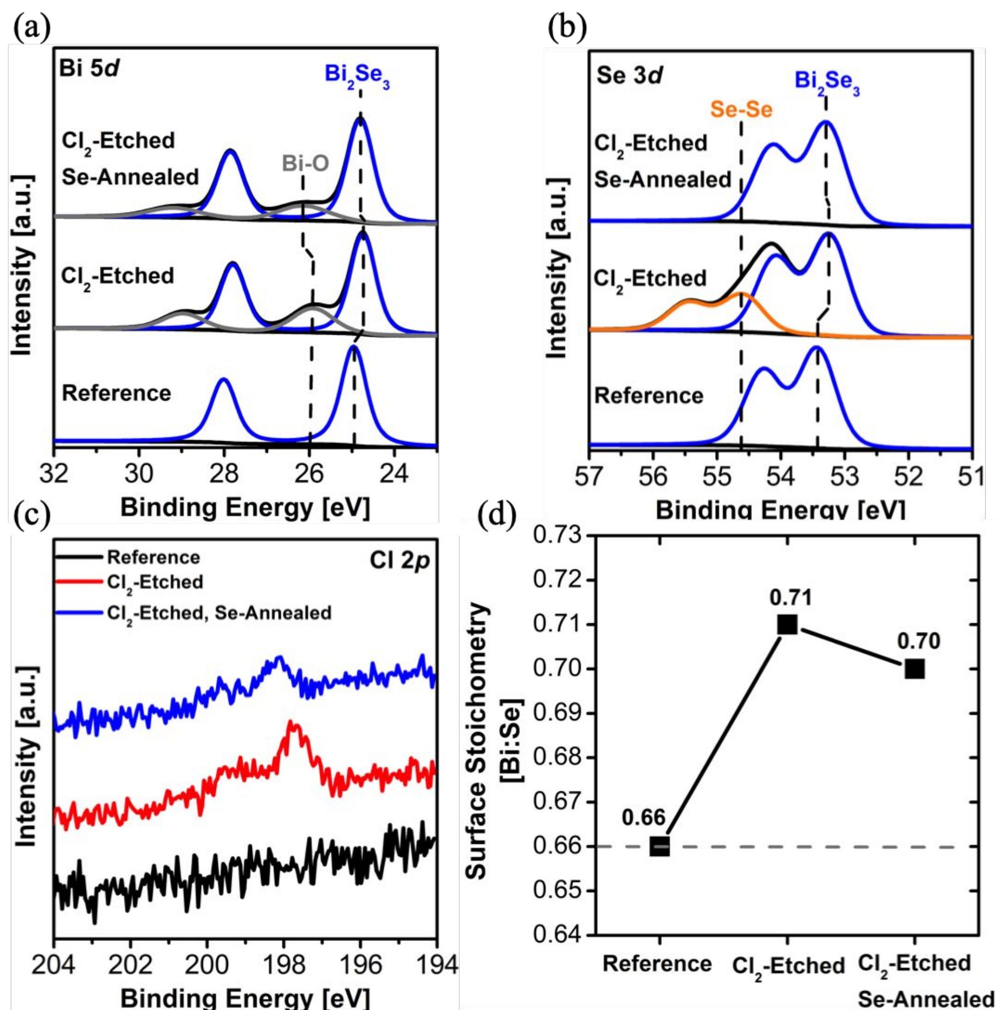

Figure 8: Fitted XPS spectra of (a) the Bi 5*d*, (b) Se 3*d*, and (c) Cl 2*p* core levels of Bi_2Se_3 immediately after growth, after the Cl_2 ICP etch, and finally after the subsequent UHV anneal under a Se-flux. (d) Bi:Se stoichiometry extracted from XPS after each processing step.

1
2
3
4
5
6
7
8
9
10
11
12
13
14
15
16
17
18
19
20
21
22
23
24
25
26
27
28
29
30
31
32
33
34
35
36
37
38
39
40
41
42
43
44
45
46
47
48
49
50
51
52
53
54
55
56
57
58
59
60

CONCLUSION

The results presented in this paper have demonstrated the robust nature of the topologically-protected surface states of Bi_2Se_3 and provide strong motivation for its implementation in defect tolerant, next-generation nanoelectronics. He^+ sputtering induces preferential removal of Se from the surface layers, which causes n-type doping. ARPES analysis of He^+ sputtered samples indicate some surface state momentum broadening, but still the Dirac cone remains, even after heavy damage. Cl_2 etches exhibit chemistry changes resulting in partially reversible Se-Se species formation and residual interstitial Cl, while SF_6 etches Bi_2Se_3 to form insulating BiF_3, essentially rendering that etch chemistry unusable. Once again, the Dirac cone remains for the Cl-etched samples despite the chemical changes. The introduction, post-etch, of low-temperature Se anneals (simply through annealing or through the utilization of a Se capping layer) helps to “heal” Se vacancies and surface chemistry changes. These results confirm the defect tolerance of the topologically protected surface states to physical and chemical surface changes.

1
2
3
4
5
6
7
8
9
10
11
12
13
14
15
16
17
18
19
20
21
22
23
24
25
26
27
28
29
30
31
32
33
34
35
36
37
38
39
40
41
42
43
44
45
46
47
48
49
50
51
52
53
54
55
56
57
58
59
60

ASSOCIATED CONTENT

AUTHOR INFORMATION

Corresponding Author

** Corresponding author email:* chinkle@nd.edu

Author Contributions

+ A. T. Barton and L. A. Walsh have contributed equally to this work.

Funding Sources

This work was supported in part by the National Science Foundation (NSF) through ECCS award numbers 1917025 and 1802166. This work was also supported in part by NEWLIMITS, a center in nCORE, a Semiconductor Research Corporation (SRC) program sponsored by NIST through award number 70NANB17H041. This work was also supported in part by the European Union's Horizon 2020 research and innovation program under the Marie Skłodowska-Curie grant agreement No 713567 and a

research grant from Science Foundation Ireland (SFI) under Grant Number SFI/12/RC/2278. Use of the Stanford Synchrotron Radiation Light Source, SLAC National Accelerator Laboratory, was supported by the U.S. Department of Energy, Office of Science, Office of Basic Energy Sciences under Contract No. DE-AC02-76SF00515.

ACKNOWLEDGMENT

The authors thank Dr. Donghui Lu and Dr. Makoto Hashimoto for their assistance with ARPES measurements at the SSRL beamline 5-4. The authors thank Profs. William Vandenberghe and Massimo Fischetti for useful discussions.

REFERENCES

1. Moore, J., Topological Insulators: The Next Generation. *Nat. Phys.* **2009**, 5, 378-380.

2. Hasan, M. Z.; Kane, C. L. Colloquium: Topological Insulators. *Rev. Mod. Phys.* **2010**, 82, 3045– 3067.

3. Moore, J. E., The Birth of Topological Insulators. *Nature* **2010**, 464, 194-198.

4. Walsh, L. A.; Hinkle, C. L., Van Der Waals Epitaxy: 2D Materials and Topological Insulators. *Appl. Mater. Today* **2017**, 9, 504-515.

5. Fu, L.; Kane, C. L.; Mele, E. J., Topological Insulators in Three Dimensions. *Phys. Rev. Lett.* **2007**, 98, 106803.

6. Walsh, L. A.; Green, A. J.; Addou, R.; Nolting, W.; Cormier, C. R.; Barton, A. T.; Mowll, T. R.; Yue, R.; Lu, N.; Kim, J.; Kim, M. J.; LaBella, V. P.; Ventrice Jr., C. A.; McDonnell, S.; Vandenberghe, W. G.; Wallace, R. M.; Diebold, A.; Hinkle, C. L., Fermi Level Manipulation through Native Doping In the Topological Insulator Bi_2Se_3. *ACS Nano* **2018**, 12, 6310-6318.

7. Vandenberghe, W. G.; Fischetti, M. V., Imperfect Two-Dimensional Topological Insulator Field-Effect Transistors. *Nat. Commun.* **2017**, 8, 14184.

8. Liu, Q.; Liu, C. X.; Xu, C. K.; Qi, X. L.; Zhang, S. C., Magnetic Impurities on the Surface of a Topological Insulator. *Phys. Rev. Lett.* **2009**, 102, 156603.

9. Brahlek, M.; Koirala, N.; Salehi, M.; Moon, J.; Zhang, W.; Li, H.; Zhou, X.; Han, M. G.; Wu, L.; Emge, T.; Lee, H. D.; Xu, C.; Rhee, S. J.; Gustafsson, T.; Armitage, N. P.; Zhu, Y.; Dessau, D. S.; Wu, W. D.; Oh, S., Disorder-Driven Topological Phase Transition in Bi_2Se_3 Films. *Phys. Rev. B* **2016**, 94, 165104.

10. Queiroz, R.; Landolt, G.; Muff, S.; Slomski, B.; Schmitt, T.; Strocov, V. N.; Mi, J.; Iversen, B. B.; Hofmann, P.; Osterwalder, J.; Schnyder, A. P.; Dil, J. H., Sputtering-Induced Re-Emergence of the Topological Surface State in Bi_2Se_3. *Phys. Rev. B* **2016**, 93, 165409.

11. Brahlek, M.; Kim, Y. S.; Bansal, N.; Edrey, E.; Oh, S. Surface Versus Bulk State in Topological Insulator Bi_2Se_3 Under Environmental Disorder. *Appl. Phys. Lett.* **2011**, 99, 012109.

12. Park, H.; Chae, J.; Jeong, K.; Choi, H.; Jeong, J.; Kim, D.; Cho, M. H. Disorder-Induced Decoupled Surface Transport Channels in Thin Films of Doped Topological Insulators. *Phys. Rev. B* **2018**, 98, 045411.

13. Hatch, R. C.; Bianchi, M.; Guan, D.; Bao, S.; Mi, J.; Iversen, B. B.; Nilsson, L.; Hornekaer, L.; Hofmann, P., Stability of the Bi_2Se_3(111) Topological State: Electron-Phonon and Electron-Defect Scattering. *Phys. Rev. B* **2011**, 83, 241303(R).

14. Patil, C. T. Cl_2/Ar Based Dry Etching of GaCrN Using Inductively Coupled Plasma. *RSC Adv.* **2016**, 6, 68619-68626.

15. Park, H. J.; Ra, H. W.; Song, K. S.; Hahn, Y. B., Inductively Coupled Plasma Etching of Ta, Co, Fe, NiFe, NiFeCo, and MnNi with Cl_2/Ar Discharges. *Korean J. Chem. Eng.* **2004**, 21: 1235-1239.

16. Pearton, S. J.; Norton, D. P. Dry Etching of Electronic Oxides, Polymers, and Semiconductors. *Plasma Proc. Polym.* **2005**, 2, 16-37.

17. Walsh, L. A.; Yue, R.; Wang, Q.; Barton, A. T.; Addou, R.; Smyth, C. M.; Zhu, H.; Kim, J.; Colombo, L.; Kim, M. J.; Wallace, R. M.; Hinkle, C. L., WTe_2 Thin Films Grown by Beam-Interrupted Molecular Beam Epitaxy. *2D Mat.* **2017,** 4, 025044.

1
2
3
4
5
6
7
8
9
10
11
12
13
14
15
16
17
18
19
20
21
22
23
24
25
26
27
28
29
30
31
32
33
34
35
36
37
38
39
40
41
42
43
44
45
46
47
48
49
50
51
52
53
54
55
56
57
58
59
60

18. Lee, W. S.; Vishik, I. M.; Lu, D. H.; Shen, Z.-X.; A Brief Update of Angle-Resolved Photoemission Spectroscopy on a Correlated Electron System. *J. Phys.: Cond. Matt.* **2009,** 21, 164217.

19. Walsh, L. A.; Smyth, C. M.; Barton, A. T.; Wang, Q.; Che, Z.; Yue, R.; Kim, J.; Kim, M. J.; Wallace, R. M.; Hinkle, C. L., Interface Chemistry of Contact Metals and Ferromagnets on the Topological Insulator Bi_2Se_3. *J. Phys. Chem. C* **2017**, 121 23551–23563.

20. Wallace, R. M., In-Situ Studies of Interfacial Bonding of High-k Dielectrics for CMOS Beyond 22nm. *ECS Trans.* **2008,** 16, 255-271.

21. Moulder, J. F., Handbook of X-ray Photoelectron Spectroscopy: A Reference Book of Standard Spectra for Identification and Interpretation of XPS Data Physical Electronics. *Physcial Electronics*, 1995.

22. Herrera-Gomez, A.; Hegedus, A.; Meissner, P. L. Chemical Depth Profile of Ultrathin Nitrided SiO_2 Films. *Appl. Phys. Lett.* **2002**, 81, 1014– 1016.

1
2
3
4
5
6
7
8
9
10
11
12
13
14
15
16
17
18
19
20
21
22
23
24
25
26
27
28
29
30
31
32
33
34
35
36
37
38
39
40
41
42
43
44
45
46
47
48
49
50
51
52
53
54
55
56
57
58
59
60

23. Addou, R.; Smyth, C. M.; Noh, J. Y.; Lin, Y. C.; Pan, Y.; Eichfeld, S. M.; Fölsch, S.; Robinson, J. A.; Cho, K.; Feenstra, R. M.; Wallace, R. M. One-Dimensional Metallic Edges in Atomically Thin WSe_2 Induced by Air Exposure. *2D Mat.* **2018**, 5, 025017.

24. Zhang, Y.; Evans, J. R. G.; Yang, S., Corrected Values for Boiling Points and Enthalpies of Vaporization of Elements in Handbooks. *J. Chem. Eng. Data* **2011,** 56, 328-337.

25. Jablonski, A.; Powell, C. J., Information Depth and the Mean Escape Depth in Auger Electron Spectroscopy and X-Ray Photoelectron Spectroscopy. *J. Vac. Sci. Tech. A* **2003**, 21, 274-283.

26. Frantzeskakis, E.; Ramankutty, S. V.; de Jong, N.; Huang, Y. K.; Pan, Y.; Tytarenko, A.; Radovic, M.; Plumb, N. C.; Shi, M.; Varykhalov, A.; de Visser, A.; van Heumen, E.; Golden, M. S., Trigger of the Ubiquitous Surface Band Bending in 3D Topological Insulators. *Phys. Rev. X* **2017,** 7, 041041.

27. Wang, J.; Zhu, B. F.; Elastic Scattering of Surface States on Three-Dimensional Topological Insulators*. Chin. Phys.* B **2013,** 22, 067301.

1
2
3
4
5
6
7
8
9
10
11
12
13
14
15
16
17
18
19
20
21
22
23
24
25
26
27
28
29
30
31
32
33
34
35
36
37
38
39
40
41
42
43
44
45
46
47
48
49
50
51
52
53
54
55
56
57
58
59
60

28. Luo, Y. R., Comprehensive Handbook of Chemical Bond Energies. *CRC Press* **2007**.

29. Dai, J.; Wang, W. B.; Brahlek, M.; Koirala, N.; Salehi, M.; Oh, S.; Wu, W., Restoring Pristine Bi_2Se_3 Surfaces with an Effective Se Decapping Process. *Nano Res.* **2015**, 8, 1222– 1228.

TABLE OF CONTENTS (TOC) GRAPHIC